Flow-Induced Beam Steering in a Single Laser Hot Spot

D. S. Montgomery, R. P. Johnson, H. A. Rose, J. A. Cobble, and J. C. Fernández

Los Alamos National Laboratory, Los Alamos, New Mexico 87545
(Received 20 September 1999)

The transmitted angular distribution of a 527 nm nearly diffraction-limited laser is measured after it propagates through a plasma with supersonic transverse flow. The laser beam is deflected by as much as 10° and exhibits bowlike features in the flow direction, which is attributed to flow-induced beam steering. The finite interaction volume allows for direct comparison with a 3D hydrodynamic simulation, which is in good agreement with details of the experiment.

Propagation of an intense laser beam through large plasmas is an important topic to laser-driven inertial confinement fusion (ICF) since effects such as filamentation and self-focusing can degrade the performance of ICF targets [1]. Recently, theoretical and experimental studies have examined laser propagation through plasmas with near-sonic transverse flow [2–6]. Supersonic plasma flow past the laser beam resonantly drives ion acoustic waves on the Mach cone, scattering power in the flow direction, resulting in beam deflection. This is an important effect for indirect drive ICF since near-sonic transverse flows can exist in regions of high laser intensity and is reported to affect capsule implosion symmetry [7].

The experimental studies to date have used laser beams with complex intensity structures, such as from a phase-aberrated beam [6], or a beam smoothed with a random phase plate (RPP) [5]. For a RPP-smoothed beam, the intensity distribution and spatial structure can be described statistically by an ensemble of laser speckles or hot spots. The dimensions of a typical hot spot within this distribution are characterized by a diffraction-limited spot of width $\sim F\lambda_0$ and length $\sim 8F^2\lambda_0$, where λ_0 is the laser wavelength ($k_0 = 2\pi/\lambda_0$), and F is the focal length to beam diameter ratio [8]. The interaction occurring within a hot spot ensemble can still be quite complex. Other instabilities, such as stimulated Raman scattering (SRS) or stimulated Brillouin scattering (SBS), may also occur in more intense hot spots within the beam [9], and can affect beam deflection through local pump depletion and profile modification. Additionally, modeling this interaction from first principles in such a large laser volume is beyond the reach of current computational tools.

In this Letter, we report a unique experimental configuration using a nearly diffraction-limited (i.e., single hot spot) laser to study flow-induced beam steering in a plasma with supersonic transverse flow. Since the laser intensity is well defined, unique regimes may be accessed where either beam steering, self-focusing, SRS, SBS, or mixtures of these are active depending on threshold conditions. The plasma is created with an additional high-energy laser beam, and the plasma conditions have been well characterized using imaging Thomson scattering [10]. The transmitted beam angular distribution, as well as SRS and SBS

backscatter, is measured. We observe beam steering up to 10° in a plasma with Mach 2 transverse flow, with insignificant ($<10^{-2}$) SRS and SBS backscatter. The transmitted beam angular distribution shows bowlike features in the direction of the flow. These experiments are compared to direct numerical simulations using a three-dimensional (3D) fluid model, and the results are in good agreement for the average deflection and for details of the angular distribution. Results obtained in this experimental configuration may be used further to benchmark and improve quantitative modeling of nonlinear beam steering, and may lead to development of accurate reduced descriptions for modeling much larger volumes.

The experiments were performed using the Trident laser facility [11]. The plasma is generated using 160 ± 10 J of 527 nm light in a 1.3 ns flattop pulse to heat a 6.7 ± 0.1 μm thick CH (parylene-N) foil [10]. The heating laser is focused normal to the target surface using an $f/6$ lens and a stripline phase plate. This produces a line focus with dimensions 100×1000 μm. The 527 nm diffraction-limited laser is delayed by 1.6 ns to interact with the plasma after the heater beam is off. The nearly diffraction-limited beam is focused using a $f/6.9$ achromatic lens, and has a FWHM spot diameter of 3.8 ± 0.15 μm. Figure 1(a) shows the measured focal distribution for the single laser hot spot in vacuum. A peak intensity of 10^{16} W/cm^2 is produced for a nominal energy of 0.8 J in a 200 ps Gaussian pulse. Note that this is $\sim\frac{1}{2}$ the peak intensity expected for an ideal focal spot due to slight
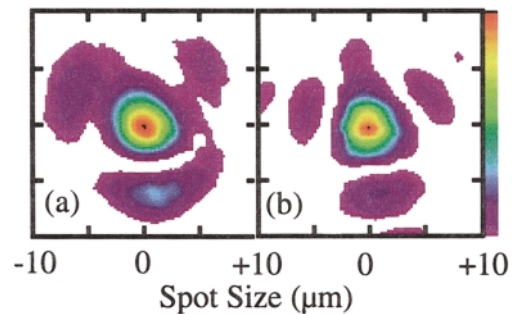

FIG. 1 (color). Focal distribution in vacuum for the single hot spot laser from (a) measurement; (b) calculation assuming $1/2\times$ the measured wave front aberration.

phase aberrations. The peak intensity is varied between 10^{14}–10^{16} W/cm² using polished, calibrated neutral density filters. The laser wave front was also measured using shearing interferometry, and the root-mean-square phase aberration is $\sim\lambda_0/5$ [10].

The single hot spot (SHS) laser is incident parallel to the surface of the target, and interacts with a ~1 mm scale quasihomogeneous plasma. The laser can be offset parallel from the target surface to vary systematically the plasma density and transverse flow. The background plasma conditions measured at the time of the SHS interaction are a density $n_e/n_{cr} \sim 0.05$ and electron temperature $T_e \approx 500$ eV, where n_{cr} is the critical density for 527 nm light ($n_{cr} \approx 4 \times 10^{21}$ cm⁻³). The measured transverse flow Mach number is $M = 2.0 \pm 0.1$. The measured transverse density and velocity gradient scale lengths are 150 and 100 μm, respectively, so that the plasma is quite homogeneous on the scale of the laser hot spot. These plasma conditions were accurately measured using imaging Thomson scattering [10] and were reproducible shot to shot.

The laser beam angular distribution is measured after it has propagated through the plasma using a diffuse scatter plate. The light scattered from the diffuser is imaged onto a 2D calibrated CCD camera. The system can detect transmitted light $\pm15°$ perpendicular to the plasma flow direction, and $-15°$ to $+30°$ in the flow direction. The angular resolution of the instrument is $0.2°$. Time-resolved spectra and reflectivity of backscattered SRS and SBS were also measured using a streaked spectrometer and calibrated photodiodes.

Figures 2(a) and 2(b) show the time-integrated transmitted beam angular distribution for intensities of 1.1×10^{15}
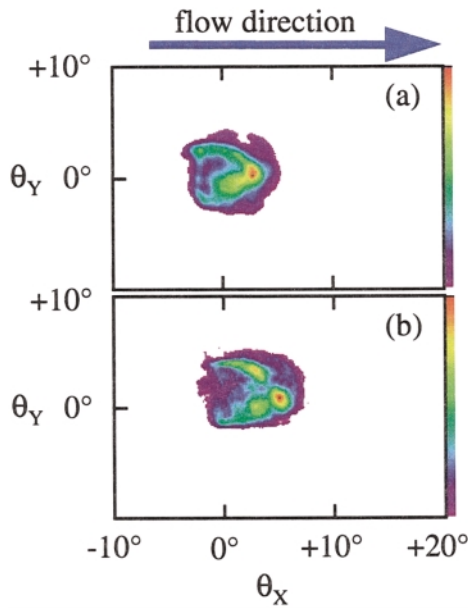
FIG. 2 (color). Measured transmitted beam angular distributions for a peak intensity of (a) 1.1×10^{15} W/cm²; (b) 2.7×10^{15} W/cm². Flow direction is in the positive θ_X direction.

and 2.7×10^{15} W/cm². The angular distribution shows an increasing deflection angle in the direction of flow as the laser intensity increases, and shows bowlike features bent toward the flow direction. A refraction angle of $6.5 \pm 0.5°$ was obtained by calculation assuming the measured density profile [10], and by direct measurement from experiments with intensity $<5 \times 10^{14}$ W/cm². This angle was subtracted from the measured angular distribution to determine the contribution from the nonlinear flow-induced beam deflection alone. For the experiments in Figs. 2(a) and 2(b), the SRS time-integrated reflectivity was $<10^{-3}$, and the SBS reflectivity was $<10^{-5}$. For cases with peak intensity exceeding 4×10^{15} W/cm², SRS was $\sim10^{-2}$, and SBS was $<10^{-3}$. Other details of the SRS and SBS will be reported in future publications.

The bowlike features in the transmitted beam angular distribution may be qualitatively explained as follows: parts of the beam "downstream" relative to "upstream" parts of the beam are destabilized, and beam power is redistributed toward the downstream side [12]. At the extreme angles ($\theta_Y \approx \pm4°$) perpendicular to the flow, there is less power in the beam compared to $\theta_Y \sim 0$, giving rise to a more intense distribution centered at $\theta_Y \sim 0$ than for larger θ_Y.

We have modeled the experimental results using a 3D fluid model, which treats paraxially only the forward going light wave [2]. The model was modified to incorporate a nonlocal electron conductivity based on linearized Fokker-Planck solutions [13]. This model is used in its simplified quasistatic limit, which assumes that the temperature fluctuation, δT, responds instantly to the local heating rate, which is proportional to the local laser intensity. This is justified since the thermal relaxation rate, $\gamma_T = (2/3)(\kappa/n_e)k^2$ is much larger than the acoustic frequency, $c_s k$, and the laser intensity varies no faster than an acoustic time scale. Although the thermal conductivity κ is greatly reduced [13] compared to the Spitzer-Härm value, κ_{SH}, $\kappa \approx \kappa_{SH}/(30k\lambda_e)^{4/3}$, the ratio $\gamma_T/c_s k$ is still large compared to unity for $k\lambda_e = O(1)$. Here, the temperature fluctuation wave number is estimated by $k \approx k_0/F$, and the electron stopping length is given by $\lambda_e = (Z_{eff}/3)\sqrt{[2/\pi(Z_{eff}+1)]}(v_e/\nu_{ei})$, where Z_{eff} is the effective charge state, v_e is the electron thermal velocity, and ν_{ei} is the electron-ion collision rate.

The hydrodynamic response may also be simplified. Since $M = 2$, and the magnitude of the density response $\delta n/n_0$ is less than unity in the cases considered, it follows that [4] even in the absence of strong acoustic wave damping, the flow remains supersonic as it passes the hot spot, with no possibility of a shock wave. A linearized hydrodynamic response is therefore used. The combination of linearized hydro and instantaneous thermal response implies that the density responds as if the plasma were isothermal but with the ponderomotive potential augmented by the factor $1 + \frac{1}{5}(1/k\lambda_D)^2(\nu_{ei}/\omega_p)^2(30k\lambda_e)^{4/3}$, where λ_D is the electron Debye length, and ω_p is the electron

plasma frequency. The thermal contribution is several times larger than the ponderomotive (the "1" term) for $k \approx k_0/F$ and for the background temperatures considered here. This is an important simplification because it is known that the ponderomotive force is also modified significantly in this regime [14], but we estimate that it is still a small correction to the thermal effect. Using this model, a maximum $\delta T/T \sim 0.26$ is calculated for a simulation at 2.3×10^{15} W/cm^2 and the plasma conditions given below.

The background conditions for these simulations are a homogeneous CH plasma with $n_e/n_{cr} = 0.05$, $T_e = 500$ eV, and $M = 2$ transverse to the laser propagation direction. The simulation has periodic boundary conditions in the x (flow) and y (perpendicular) directions, and the laser propagates in the z direction. The simulation box size was typically $122F/k_0 \times 80F/k_0 \times 223F^2/k_0$, and the grid size $128 \times 64 \times 600$ in the (x, y, z) directions. The laser conditions were $\lambda_0 = 527$ nm, 200 ps Gaussian temporal pulse shape, and $f/7$ focusing optic. A phase aberration model was used which was consistent with both the measured focal spot and measured wave front. Because of uncertainties in the measured phase, simulations were performed which assumed either the full measured aberration, $1/2\times$, or $1/4\times$ the measured aberration to bracket the experimental conditions. The calculated focal distribution (in vacuum) is shown in Fig. 1(b) for $1/2\times$ phase aberration. Apart from the linearized treatment for thermal effects, these simulations are thought to incorporate much of the interaction physics in the experiment since the SRS and SBS reflectivities are quite low for intensities $<4 \times 10^{15}$ W/cm^2. Therefore, is it reasonable to make direct comparisons between the experimental and simulation results for the low intensity cases. The large SRS reflectivity for intensities $\sim 8 \times 10^{15}$ W/cm^2 is expected to contribute significantly to density perturbations within the hot spot, which is beyond the range of validity for this model.

Figures 3(a) and 3(b) show the simulated time-integrated transmitted beam distributions for 7.5×10^{14} and 1.5×10^{15} W/cm^2 using $1/2\times$ aberration. The bowlike shape observed in the experiments is qualitatively reproduced in the model. It is important to note that, while the thermal model may not be physically complete, the thermal response is necessary to reproduce qualitatively the angular distributions observed in the experiment. Figure 3(c) shows the simulated transmitted beam distribution for 1.5×10^{15} W/cm^2 using an isothermal (ponderomotive only) plasma response with $1/2\times$ aberration. For this simulation, the transmitted energy is only slightly redistributed within the original beam cone, and does not produce a bowlike feature as observed experimentally.

Figure 4 shows the centroid of the deflected transmitted beam in the flow (θ_X) direction versus peak laser intensity for the experiments and simulations. Simulations were performed with the full thermal response and an isothermal
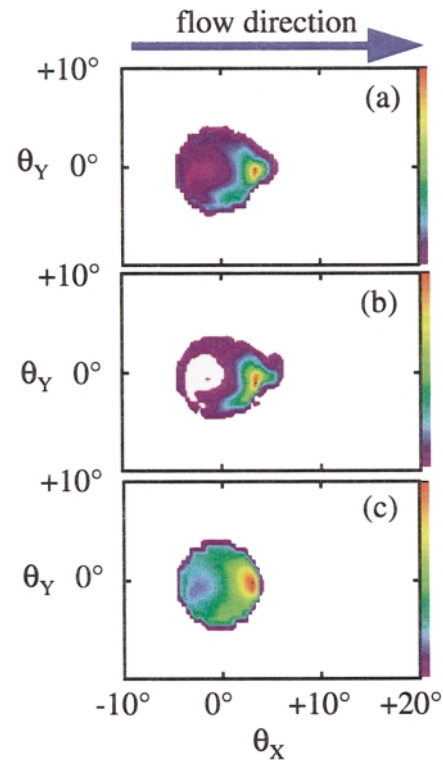

FIG. 3 (color). Simulated transmitted beam angular distributions from the model assuming $1/2\times$ phase aberration and using the full thermal response for (a) $I = 7.5 \times 10^{14}$ W/cm^2; (b) $I = 1.5 \times 10^{15}$ W/cm^2; (c) transmitted beam angular distribution using the isothermal plasma model for $I = 1.5 \times 10^{15}$ W/cm^2.

response. The input aberration was varied between $1/4\times$ and the full measured aberration. The deflection was remarkably insensitive to changes in aberration, so only results with $1/2\times$ aberration are shown. For lower laser intensities, beam deflection in the isothermal model is $\sim \frac{1}{5}$ that of the full thermal model. However at higher intensities, the latter's deflection is strongly saturated, while
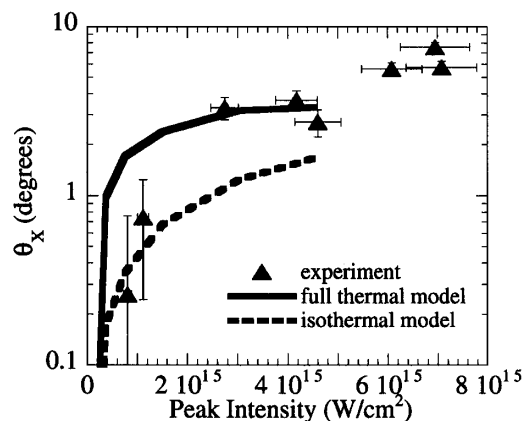

FIG. 4. Plot of deflected beam centroid versus peak intensity for experiments (triangles), 3D fluid model with full thermal response (solid line), and isothermal response (dashed line).

the former is not, and the two predictions become comparable. Time-dependent intensity and ion inertia create a spatially sinuous density channel in the simulations. In the full model at the larger intensities, it is deep enough to trap the light over a large enough extent such that the beam deflection peaks near best focus and then, following the curved channel, diminishes with further propagation. This is a temporally and spatially unstable process that is sensitive to the beam's small aberration. Simulations with a perfect (nonaberrated) beam yield a peak deflection at about 3×10^{15} W/cm^2 which decreases for higher intensity, while the slight aberration present in the actual beam yields a model whose deflection peaks at about 5×10^{15} W/cm^2. A small aberration appears to allow the beam to escape the density channel so that the peak deflection near best focus is more representative of that in the transmitted beam near field. Other details of these simulations will be reported in a future publication.

Figures 5(a) and 5(b) show angular profiles taken parallel and perpendicular to the flow direction for an intensity of 2.7×10^{15} W/cm^2 for the experiment, and for the thermal response model at 3×10^{15} W/cm^2. The profiles are normalized to the maximum transmission. The comparisons show that the overall shape of the transmitted angular distributions agree quite well in the parallel and perpendicular flow directions. However, the simulations underestimate the relative amount of energy scattered into the "bows" [Fig. 5(b)]. More energy is scattered into the bows for the experiment compared to the model, which contributes to a lower measured centroid for the experiment compared to the model. This explains why the measured centroids are lower than the thermal model simulations at the lowest intensities. A simple centroid is insensitive to details in the angular distribution, and therefore should not be used as the only benchmark to compare with experimental data.

Finally, it is interesting to note that significant beam deflection is observed for *supersonic* transverse flow as predicted by theory [2], not only for $M \approx 1$. The simulation results are in good quantitative agreement with the experiments for the deflected beam centroid, and are in good qualitative agreement for the details of the angular distribution, despite the simplifications made in the model. This good agreement is encouraging for hopes of eventually developing a quantitative predictive capability for laser plasma instabilities.

In conclusion, we have used a single laser hot spot to study nonlinear beam deflection in a plasma with supersonic transverse flow. We observe beam deflection up to 10° for Mach ~2. The transmitted angular distribution shows interesting bowlike structures in the direction of plasma flow. The plasma and laser conditions are well characterized and the interaction volume is nearly mini-
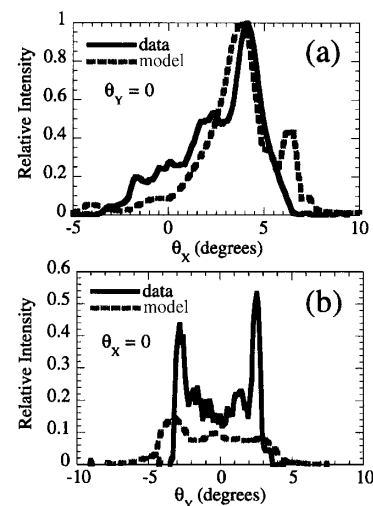

FIG. 5. Comparison of transmitted beam angular distribution [see Fig. 2(b)] for experiment at $I = 2.7 \times 10^{15}$ W/cm^2 (solid lines) and simulation (dashed lines). Model profiles taken from simulation with full thermal response for $I = 3 \times 10^{15}$ W/cm^2. Angular distribution profiles are shown at (a) $\theta_Y = 0$ in the θ_X direction; at (b) $\theta_X = 0$ in the θ_Y direction.

mal for the laser optic, both of which facilitate direct comparison with numerical simulations that incorporate first-principles models.

[1] J. Lindl, Phys. Plasmas **2**, 3933 (1995).
[2] H. A. Rose, Phys. Plasmas **3**, 1709 (1996).
[3] D. E. Hinkel, E. A. Williams, and C. H. Still, Phys. Rev. Lett. **77**, 1298 (1996).
[4] S. Ghosal and H. A. Rose, Phys. Plasmas **4**, 2376 (1997).
[5] J. D. Moody *et al.,* Phys. Rev. Lett. **77**, 1294 (1996).
[6] P. E. Young *et al.,* Phys. Rev. Lett. **81**, 1425 (1998).
[7] N. Delamater *et al.,* Phys. Plasmas **3**, 2022 (1996).
[8] H. A. Rose and D. F. Dubois, Phys. Fluids B **5**, 590 (1993).
[9] H. A. Rose and D. F. Dubois, Phys. Rev. Lett. **72**, 2883 (1994).
[10] D. S. Montgomery *et al.,* Laser Part. Beams **17**, 349 (1999).
[11] N. K. Moncur *et al.,* Appl. Opt. **23**, 4274 (1995).
[12] H. A. Rose and S. Ghosal, Phys. Plasmas **5**, 1461 (1998).
[13] E. M. Epperlein, Phys. Rev. Lett. **65**, 2145 (1990).
[14] A. V. Brantov *et al.,* Phys. Plasmas **5**, 2742 (1998).